Eur. Phys. J. C (2014) 74:2943
DOI 10.1140/epjc/s10052-014-2943-y

THE EUROPEAN PHYSICAL JOURNAL C

Regular Article - Theoretical Physics

Study of inflationary generalized cosmic Chaplygin gas for standard and tachyon scalar fields

M. Sharif[a], **Rabia Saleem**[b]

Department of Mathematics, University of the Punjab, Quaid-e-Azam Campus, Lahore 54590, Pakistan

Received: 13 February 2014 / Accepted: 8 June 2014 / Published online: 5 July 2014

Abstract We consider an inflationary universe model in the context of the generalized cosmic Chaplygin gas by taking the matter field as standard and tachyon scalar fields. We evaluate the corresponding scalar fields and scalar potentials during the intermediate and logamediate inflationary regimes by modifying the first Friedmann equation. In each case, we evaluate the number of e-folds, scalar as well as tensor power spectra, scalar spectral index, and the important observational parameter, the tensor–scalar ratio in terms of inflation. The graphical behavior of this parameter shows that the model remains incompatible with WMAP7 and Planck observational data in each case.

1 Introduction

A combination of different cosmic probes like type Ia supernova, the large scale structure (LSS), cosmic microwave background (CMB), and WMAP confirmed that our universe is experiencing accelerating expansion [1,2]. Little is known about the origin of this cosmic stage, which may be due to dark energy (DE) (with large negative pressure). It fills two-third of the whole cosmic energy and the remaining portion is almost as a whole occupied by the dark matter (DM). A tiny constant Λ is the simplest identification of DE, which suffers from fine-tuning and cosmic coincidence issues. The dynamical nature of DE is variously assigned to scalar field models (quintessence, phantom, k-essence etc.) [3–6] and interacting DE models (Chaplygin gas (CG), holographic DE, Ricci DE etc.) [7–9].

The Chaplygin gas (a unification of DE and DM) is considered to be an interesting alternative description of accelerating expansion. It has negative pressure obeying the equation of state (EoS) $P=-\frac{A}{\rho}$, $A>0$ and having a positive speed of sound, which is a powerful tool to discriminate between various DE models. The velocity of sound approaches the velocity of light for late times, while it is negligibly small for early times. The energy density of CG smoothly varies from the matter dominated era to a constant point, i.e., Λ cold DM (ΛCDM) in the future universe [10]. Many people studied cosmology via different models of CG, like generalized CG (GCG) [11], modified CG (MCG) [12] and generalized cosmic CG (GCCG) [13], etc. Kamenshchik et al. [14] considered an FRW universe composed of CG and showed that the resulting evolution of the universe is in agreement with the current observation of cosmic acceleration.

Recently, a great amount of work has been done in investigating the inflationary universe model with a tachyon field. This field might be responsible for cosmological inflation in the early evolution of the universe due to tachyon condensation near the top of the effective scalar potential [15], which could also add some new form of cosmological DM at late times [16]. Gibbons [17] was the first who studied the cosmological implications of this rolling tachyon. It is quite natural to consider some scenarios in which inflation is driven by the rolling tachyon. The CG emerges as an effective fluid of a generalized d-brane in a $(d+1,1)$ spacetime, where the action can be written as a generalized Born–Infeld action [18]. These models (CG and tachyon) have extensively been studied in the literature [19–23]. In a Chaplygin inspired inflationary universe model, the standard inflation field usually drives inflation where the energy density can be extrapolated for obtaining a successful inflation period [24]. Del Campo and Herrera [25,26] studied warm-Chaplygin and tachyon-Chaplygin inflationary universe models. Monerat et al. [27] explored the dynamics of the early universe and initial conditions for an inflationary model with radiation and CG.

The standard cosmology explains the observation of CMB radiation in an elegant way but the early phase of the universe is still facing some long-standing issues like the horizon problem, flatness, numerical density of monopoles, and the ori-

[a] e-mail: msharif.math@pu.edu.pk

[b] e-mail: rabiasaleem1988@yahoo.com

gin of fluctuations [28,29]. The inflationary models present a better description of the early universe, which also provide the most compelling solution of these problems. Inflation can provide an elegant mechanism to explain the causal interpretation of the origin of the observed anisotropy of CMB and the inhomogeneity for structure formation. Scalar field models composed of kinetic and potential terms coupled to gravity produce a dynamical framework and act as a source for inflation. These models have the ability to interpret the distribution of LSS and the observed anisotropy of CMB radiations comprehensively in the inflationary era [30].

The inflationary era is divided into slow-roll and reheating epochs. During the slow-roll approximation, the universe inflates as the interactions between inflatons and other fields become negligibly small and the potential energy dominates the kinetic energy. After this period, the universe enters the last stage of inflation, i.e., the reheating era, in which the kinetic and potential energies are comparable. Here the inflation starts to oscillate around the minimum of its potential while losing its energy to massless particles. The inflationary model is usually discussed in the intermediate and logamediate scenarios.

During the intermediate era, the universe expands at a rate slower than the standard de Sitter inflation but faster than power-law inflation [31]. Setare and Kamali [32] have discussed warm vector inflation in this scenario for the FRW model and proved that the results are compatible with the WMAP7 data [33,34]. The same authors [35] also dealt with warm inflation using gauge fields in the intermediate as well as the logamediate scenarios. In recent papers [36,37], we have studied the warm vector inflation and warm gauge-flation in a locally rotationally symmetric Bianchi type I universe model and verified their compatibility with WMAP7 data.

The study of the inflationary epoch with intermediate and logamediate scale factors leads to over-lasting forms of the potential which agree with tachyon potential properties. Moreover, the study of warm inflation as a mechanism leads to an end for standard and tachyon inflation. This motivated us to consider an inflationary model with these two potentials. Recently, Herrera et al. [38] studied an intermediate GCG inflationary universe model with standard as well as tachyon scalar fields and checked its compatibility with WMAP7 data. Since GCCG is less constrained as compared to MCG and GCG and is capable of adapting itself to any domain of cosmology, depending upon the choice of parameters. Thus it has a more universal character and the big-rip singularity can easily be avoided in this model. These generalizations of CG can lead to significant changes in the early universe. It would be interesting to check the behavior of the inflationary universe with GCCG using the standard and tachyon scalar fields during the intermediate as well as logamediate epochs. This work can recover all the previous existing models of CG.

The paper is arranged in the following format. In the next section, we modify the first Friedmann equation and find solutions of standard and tachyon scalar fields as well as their corresponding potentials. We also provide the slow-roll parameters, number of e-folds, scalar and tensor power spectra, scalar spectral index, and tensor–scalar ratio. In Sect. 3, we develop our model in intermediate and logamediate inflation with both types of scalar fields. We conclude our discussion in the last section.

2 Inflation with standard and tachyon scalar fields

In this section, we modify the first Friedmann equation in the context of the GCCG inflationary universe model. We choose standard and tachyon scalar fields as the matter content of this universe and calculate both scalar fields and their corresponding potentials. We also formulate some important perturbed parameters.

González-Diaz [13] introduced the GCCG model in such a way that the resulting models can be made stable and physical, even when the vacuum fluid satisfies the phantom energy condition. It has the following exotic EoS:

$$P = -\rho^{-\alpha}[C + (\rho^{1+\alpha} - C)^{-\omega}], \tag{1}$$

where $C = \frac{A}{1+\omega} - 1$, A is an either positive or negative constant, α is any positive constant and $-l < \omega < 0, l > 1$. This EoS reduces to the GCG model as $\omega \to 0$. The corresponding energy density is obtained by integrating the energy conservation equation of the GCCG as follows:

$$\rho = \left[C + \left(1 + \frac{B}{a^{3(1+\alpha)(1+\omega)}}\right)^{\frac{1}{1+\omega}}\right]^{\frac{1}{1+\alpha}}, \tag{2}$$

with the scale factor a, and B is the integration constant. The gravity dynamics during inflation leads to a modification of the first Friedmann equation [18]:

$$H^2 = \frac{\kappa}{3(1+\omega)}\left[C + \rho_\phi^{(1+\alpha)(1+\omega)}\right]^{\frac{1}{1+\alpha}}, \tag{3}$$

where $\kappa = \frac{8\pi}{m_{\mathrm{p}}^2}$, m_{p} is the reduced Planck mass and ρ_ϕ is the energy density of the scalar field. This modification is dubbed Chaplygin inspired inflation.

We take two types of scalar fields for ρ_ϕ, i.e., standard and tachyon scalar fields. The energy conservation of a scalar field is

$$\dot{\rho}_\phi + 3H(\rho_\phi + P_\phi) = 0, \tag{4}$$

where the associated standard energy density and pressure are given as

$$\rho_\phi = \frac{\dot\phi^2}{2} + V(\phi), \quad P_\phi = \frac{\dot\phi^2}{2} - V(\phi).$$

Using ρ_ϕ and P_ϕ, the above equation is equivalent to the equation of motion of the standard scalar field as follows:

$$\ddot\phi + 3H\dot\phi + V'(\phi) = 0, \tag{5}$$

where $'$ denotes the derivative with respect to ϕ. Equations (3) and (4) yield

$$\dot\phi^2 = -\left(\frac{2\dot H}{\kappa}\right)\left(\frac{3H^2}{\kappa}\right)^{\alpha}\left(\frac{3H^2}{\kappa}\right)^{(1+\alpha)\psi} \times\left[1-\frac{A}{(1+\omega)}\left(\frac{\kappa}{3H^2}\right)^{1+\alpha}\right]^{\psi}, \tag{6}$$

where $\psi = \left[\frac{1}{(1+\alpha)(1+\omega)} - 1\right]$. The scalar potential is obtained by substituting ρ_ϕ from (3) and $\dot\phi^2$ from (6) in the formula for the energy density of the standard scalar field as follows:

$$V(t) = (1+\omega)\left[\left(\frac{3H^2}{\kappa}\right)^{1+\alpha} - \frac{A}{(1+\omega)}\right]^{\psi+1} + \left[\frac{\dot H}{\kappa}\left(\frac{3H^2}{\kappa}\right)^{\alpha+(1+\alpha)\psi}\left[1-\frac{A}{(1+\omega)}\left(\frac{\kappa}{3H^2}\right)^{1+\alpha}\right]^{\psi}\right]. \tag{7}$$

The above two solutions reduce to the typical standard inflation for $\alpha,\ A,\ \omega \to 0$, the pure CG model for $\alpha,\ \omega \to 0$, and the GCG model for $\omega \to 0$ [39–42].

The energy density and pressure of the tachyon field are

$$\rho_\phi = \frac{V(\phi)}{\sqrt{1-\dot\phi^2}}, \quad P_\phi = V(\phi)\sqrt{1-\dot\phi^2}. \tag{8}$$

Using Eq. (4), we obtain the corresponding equation of motion,

$$\frac{\ddot\phi}{1-\dot\phi^2} + 3H\dot\phi + \frac{V'(\phi)}{V(\phi)} = 0. \tag{9}$$

Equations (3) and (9) provide the time derivative of the tachyon field as follows:

$$\dot\phi^2 = -\left(\frac{2\dot H}{\kappa}\right)\left(\frac{3H^2}{\kappa}\right)^{\alpha}\frac{1}{(1+\omega)}\left[\left(\frac{3H^2}{\kappa}\right)^{1+\alpha} - \frac{A}{1+\omega}\right]^{-1}. \tag{10}$$

Using the above equation with (3) in ρ_ϕ given in (8), we have the tachyon potential

$$V(t) = (1+\omega)^{\frac{1}{2}} \times\sqrt{1+\frac{2\dot H}{\kappa}\left(\frac{3H^2}{\kappa}\right)^{\alpha}\frac{1}{(1+\omega)}\left[\left(\frac{3H^2}{\kappa}\right)^{1+\alpha} - \frac{A}{1+\omega}\right]^{-1}} \times\left[\left(\frac{3H^2}{\kappa}\right)^{1+\alpha} - \frac{A}{(1+\omega)}\right]^{\psi+1}. \tag{11}$$

The dimensionless slow-roll parameters ϵ, η, and number of e-folds are defined as

$$\epsilon = -\frac{\dot H}{H^2}, \quad \eta = -\frac{\ddot H}{H\dot H}, \quad N = A\int_{t_1}^{t_2} H\,dt; \quad A > 0, \tag{12}$$

where t_1 and t_2 are the starting and ending cosmic time of the inflationary era.

Now we define scalar and tensor power spectra for the GCCG inflationary model with the standard and tachyon scalar fields. The power spectrum as a function of wave number (k) is the basic tool to quantify the fluctuations' variance produced by the inflatons. In order to calculate scalar perturbation, a gauge invariant quantity, $\zeta = H + \frac{\delta\rho}{\dot\rho}$, is introduced [43]. This quantity almost remains constant on super-horizon scales but reduces to a curvature perturbation on a slice of uniform density. This fundamental characteristic is a consequence of stress-energy conservation and independent of the gravitational dynamics which keeps it unchanged in the Chaplygin inflationary model [44]. Thus the power spectrum corresponds to the curvature spectrum and can be written as $\mathcal{P}_\mathcal{R} = \langle\zeta^2\rangle$ [38]. Since the curvature perturbations act as a comoving curvature perturbation on the slices of uniform density, for the spatially flat gauge fields we have [45]

$$\mathcal{P}_\mathcal{R} \simeq H^2\frac{(\delta\phi)^2}{(\dot\phi)^2}; \quad |\delta\phi| = \frac{H}{2\pi} \Rightarrow \mathcal{P}_\mathcal{R} \simeq \frac{H^4}{4\pi^2\dot\phi^2}. \tag{13}$$

The scalar power spectrum for a tachyon field using the slow-roll approximation ($(\dot\phi)^2 << V(\phi)$) has the form [46]

$$\mathcal{P}_\mathcal{R} \simeq \left(\frac{H^2}{2\pi\dot\phi}\right)^2\frac{1}{Z_s}; \quad Z_s = V(1-(\dot\phi)^2)^{-\frac{3}{2}} \approx V(\phi). \tag{14}$$

The tensor perturbation generating gravitational waves and the scalar spectral index, n_s, are defined as

$$\mathcal{P}_g = 8\kappa\left(\frac{H}{2\pi}\right)^2, \quad n_s - 1 = -\frac{d\ln\mathcal{P}_\mathcal{R}(k)}{d\ln k}. \tag{15}$$

The tensor–scalar ratio (an observable quantity) for both standard and tachyon scalar fields, respectively, is

$$r=\frac{\mathcal{P}_g}{\mathcal{P}_{\mathcal{R}}}=8\kappa\left(\frac{\dot{\phi}}{H}\right)^2,\quad r=8\kappa\left(\frac{\dot{\phi}}{H}\right)^2 V. \tag{16}$$

According to the observations of WMAP + BAO (baryon acoustic oscillations) + SN, the scalar spectral index and perturbed scalar power spectrum are constrained to $0.96 \leq n_s \leq 1.002$ (95 % C.L.) and $\mathcal{P}_{\mathcal{R}}(k_0 = 0.002\ \mathrm{Mpc}^{-1}) = (2.445 \pm 0.096) \times 10^{-9}$, respectively [30], while the tensor power spectrum cannot be constrained directly. In this context, a physically acceptable range of the tensor–scalar ratio is determined, i.e., $r < 0.36$ (95 % C.L.), which represents the expanding universe.

3 Intermediate and logamediate inflation

Here, the GCCG inflationary universe model is developed in the intermediate and logamediate eras using the standard and tachyon scalar fields. We reconstruct solutions of both fields, their potentials, and perturbed parameters (found in the above section) during the times of these two scenarios.

3.1 Standard scalar field

First, we take the standard scalar field as matter content of the inflationary universe and discuss in the intermediate as well as logamediate scenarios.

3.1.1 Intermediate inflation

This era is motivated by string/M theory and is one of the exact solutions of the inflationary cosmology. The 4-dimensional Gauss–Bonnet interaction with dynamical dilatonic scalar coupling leads to an intermediate form of the scale factor [39]

$$a(t)=a_0\exp(At^f),\quad A>0,\ 0<f<1, \tag{17}$$

where a_0 is the value of scale factor at $t = 0$. Using Eq. (17) in (6), we obtain the following solution of the standard scalar field ϕ:

$$\phi(t)-\phi_0=\frac{2\left(\frac{2}{\kappa}(Af)(1-f)\left(\frac{3(Af)^2}{\kappa}\right)^{\alpha+(1+\alpha)\psi}\right)^{\frac{1}{2}}}{f+2(f-1)\left[\alpha+(1+\alpha)\psi\right]}\times t^{\frac{f+2(f-1)[\alpha+(1+\alpha)\psi]}{2}}, \tag{18}$$

where ϕ_0 is an integration constant at $t = 0$. Without loss of generality, we can take $\phi_0 = 0$ to express the time in terms of the scalar field as

$$t=\left[\frac{\phi\left[f+2(f-1)\left[\alpha+(1+\alpha)\psi\right]\right]}{2\left(\frac{2}{\kappa}(Af)(1-f)\left(\frac{3(Af)^2}{\kappa}\right)^{\alpha+(1+\alpha)\psi}\right)^{\frac{1}{2}}}\right]^{\frac{2}{f+2(f-1)[\alpha+(1+\alpha)\psi]}}. \tag{19}$$

Using Eq. (17), the standard scalar potential (7) is as follows:

$$V(\phi)=(1+\omega)\left[\left[\frac{\phi\left[f+2(f-1)\left[\alpha+(1+\alpha)\psi\right]\right]}{2\left(\frac{2}{\kappa}(Af)(1-f)\left(\frac{3(Af)^2}{\kappa}\right)^{\alpha+(1+\alpha)\psi}\right)^{\frac{1}{2}}}\right]^{\frac{4(f-1)(1+\alpha)}{f+2(f-1)[\alpha+(1+\alpha)\psi]}}\times\left(\frac{3(Af)^2}{\kappa}\right)^{1+\alpha}-\frac{A}{1+\omega}\right]^{\psi+1}. \tag{20}$$

The slow-roll parameters and number of e-folds are found through Eq. (12) using Eq. (19). Another scalar field ϕ_1 is produced at the beginning of the inflation epoch, where $\epsilon = 1$. The standard scalar power spectrum during the intermediate era can be calculated by inserting Eq. (6) in Eq. (13) and then, using Eq. (19), it follows that

$$\mathcal{P}_{\mathcal{R}}=\frac{(Af)^3}{(1-f)}\left(\frac{\kappa}{8\pi^2}\right)\mu^{\frac{3f-2}{f}}\times\left[\mu^{\frac{2(f-1)}{f}}\left(\frac{3}{\kappa}\right)(Af)^2\right]^{-\alpha-(1+\alpha)\psi}\left[1-\frac{A}{1+\omega}\times\mu^{\frac{2(1-f)(1+\alpha)}{f}}\left(\frac{\kappa}{3(Af)^2}\right)^{1+\alpha}\right]^{-\psi}, \tag{21}$$

where $\mu=\frac{1+f(N-1)}{Af}$. Equation (15) provides P_g and n_s as a function of N, respectively:

$$\begin{aligned}n_s-1&=\frac{2-3f}{Af}\mu^{-1}+2\left[-\alpha-(1+\alpha)\psi\right]\left(\frac{f-1}{f}\right)\mu^{\frac{(1-f)}{f}}\\&\quad-\psi\left[1-\frac{A}{1+\omega}\left(\frac{\kappa}{3(Af)^2}\right)^{1+\alpha}\mu^{\frac{2(1-f)(1+\alpha)}{f}-1}\right]\\&\quad\times\left[\frac{2(f-1)(1+\alpha)}{f(1+\omega)}\left(\frac{\kappa}{3(Af)^2}\right)^{1+\alpha}\mu^{\frac{2(1-f)(1+\alpha)}{f}-1}\right],\\P_g&=\left(\frac{2\kappa}{\pi^2}\right)(Af)^2\mu^{\frac{2(f-1)}{f}}.\end{aligned} \tag{22}$$

Using Eqs. (21) and (22), the tensor–scalar ratio has the form

$$r(N)=16\left(\frac{1-f}{Af}\right)\mu^{-1}\left[\left(\frac{3}{\kappa}\right)(Af)^2\mu^{\frac{2(f-1)}{f}}\right]^{\alpha+(1+\alpha)\psi}\times\left[1-\frac{A}{1+\omega}\times\left(\frac{\kappa}{3(Af)^2}\right)^{1+\alpha}\mu^{\frac{2(1-f)(1+\alpha)}{f}}\right]^{\psi}.$$

The left panel of Fig. 1 shows increasing behavior of n_s with respect to N. The observed value of $n_s = 0.96$ corresponds to $N \approx 20$ for all values of parameters, which indicates physical

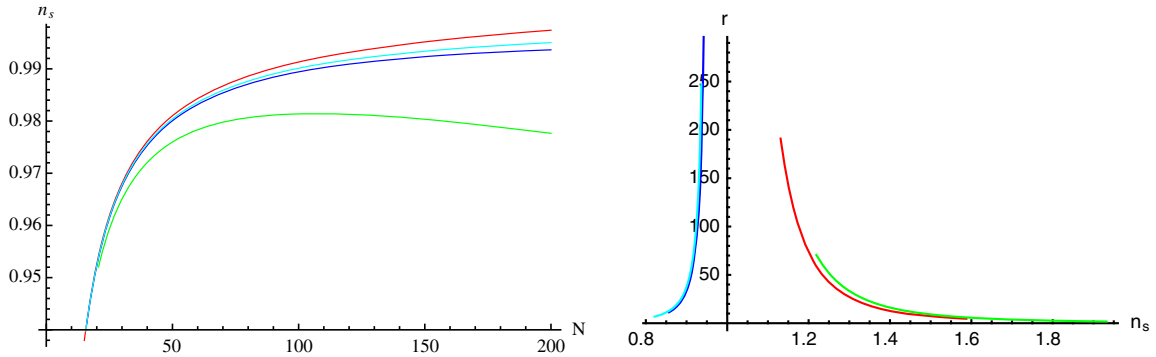

Fig. 1 *Left* n_s versus N, *right* tensor–scalar ratio versus n_s for $A = 8.225 \times 10^2$, $\alpha = 0.775$, $\omega = -0.8$, $g = \frac{1}{2}$, $k = 1$ (*red*); $A = 2.635 \times 10^2$, $\alpha = 0.81$, $\omega = -1.5$ (*green*); $A = 8.407 \times 10^2$, $\alpha = 0.85$, $\omega = -1.7$ (*blue*) and $A = 8.407 \times 10^2$, $\alpha = 0$, $\omega = 0$ (*zinc*) in the intermediate scenario

compatibility of these model parameters with WMAP7 data. The right graph of Fig. 1 shows that red and green r–n_s trajectories are decreasing, while the other two are increasing. We see that none of the cases is compatible with WMAP7 data as the observed value $0.96 \leq n_s \leq 1$ does not lie in the region $r \leq 0.36$ during the era of the intermediate scenario.

3.1.2 Logamediate inflation

The logamediate inflationary era is motivated by imposing weak general conditions on the indefinitely expanding cosmological models. It has been proved that the power spectrum is either red or blue tilted for this type of inflation. The scale factor satisfies [34]

$$a(t) = a_0 \exp[A(\ln t)^{\lambda}], \quad \lambda > 1. \tag{23}$$

For $\lambda = 1$, it is converted to power-law inflation. During logamediate inflation, Eq. (6) has the following solution:

$$\begin{aligned}\phi(t) - \phi(t_0) &= -\Xi(t)\left[\left(\frac{2}{\kappa}\right)\left(\frac{3}{\kappa}\right)^{\alpha+(1+\alpha)\psi}(A\lambda)^{1+2(\alpha+(1+\alpha)\psi)}\right]^{\frac{1}{2}} \\ &\times\left[\frac{A}{1+\omega}\left(\frac{\kappa}{3}\right)^{1+\alpha}(A\lambda)^{-2(1+\alpha)}\right]^{\frac{\psi}{2}},\end{aligned} \tag{24}$$

where $\Xi(t) = \gamma[\frac{\lambda+2\alpha(\lambda-1)}{2}, \alpha \ln t]$ (γ is the incomplete gamma function). From the above equation, t is calculated in terms of ϕ as

$$\begin{aligned}t = \Xi^{-1}\left[-\phi\left[\left(\frac{2}{\kappa}\right)\left(\frac{3}{\kappa}\right)^{\alpha+(1+\alpha)\psi}(A\lambda)^{1+2(\alpha+(1+\alpha)\psi)}\right]^{-\frac{1}{2}}\right. \\ \left.\times\left[\frac{A}{1+\omega}\left(\frac{\kappa}{3}\right)^{1+\alpha}(A\lambda)^{-2(1+\alpha)}\right]^{-\frac{\psi}{2}}\right].\end{aligned} \tag{25}$$

The corresponding Hubble parameter, the standard scalar potential, the slow-roll, as well as number of e-folds can be calculated as in the intermediate case.

The scalar and tensor perturbed parameters in terms of N can be written as

$$\begin{aligned}\mathcal{P}_{\mathcal{R}} &= \left(\frac{\kappa}{8\pi^2}\right)\left(\frac{\kappa}{3}\right)^{\alpha+(1+\alpha)\psi}\frac{(A\lambda)^{3-2(\alpha+(1+\alpha)\psi)}}{(1-\lambda)} \\ &\times\varepsilon^{\frac{3\lambda-2(\lambda-1)(\alpha+(1+\alpha)\psi)-2}{\lambda}} \\ &\times\exp\left[\left(\frac{2(\alpha+(1+\alpha)\psi)-1}{\lambda}\right)\varepsilon\right] \\ &\times\left[1-\frac{A}{1+\omega}\left(\frac{\kappa}{3(A\lambda)^2}\right)^{1+\alpha}\right. \\ &\left.\times\varepsilon^{\frac{-2(1+\alpha)}{\lambda}}\exp\left[\frac{2\varepsilon(1+\alpha)}{\lambda}\right]\right]^{-\psi}, \\ \mathcal{P}_g &= \left(\frac{2\kappa}{\pi^2}\right)(A\lambda)^2\varepsilon^{\frac{\lambda-1}{\lambda}}\exp\left[-\frac{\varepsilon}{\lambda}\right],\end{aligned}$$

where $\varepsilon = \left[\frac{N}{A} + (A\lambda)^{\frac{\lambda}{1-\lambda}}\right]$. Using $\mathcal{P}_{\mathcal{R}}$, we obtain the scalar spectral index:

$$\begin{aligned}n_s - 1 &= \left(\frac{3\lambda-2(\lambda-1)(\alpha+(1+\alpha)\psi)-2}{A\lambda}\right) \\ &\times\varepsilon^{\frac{3\lambda-2(\lambda-1)(\alpha+(1+\alpha)\psi)-2}{\lambda}} \\ &+\frac{2(\alpha+(1+\alpha)\psi-1)}{A\lambda} - \psi\left[\frac{A}{1+\omega}\left(\frac{\kappa}{3}\right)^{1+\alpha}\right. \\ &\times(A\lambda)^{-2(1+\alpha)}\varepsilon^{\frac{-2(1+\alpha)}{\lambda}} \\ &\left.\times\exp\left[\frac{2\varepsilon(1+\alpha)}{\lambda}\right]\right]\left[\varepsilon^{-1}-1\right] \\ &\times\left[1-\frac{A}{1+\omega}\left(\frac{\kappa}{3}\right)^{1+\alpha}(A\lambda)^{-2(1+\alpha)}\varepsilon^{\frac{-2(1+\alpha)}{\lambda}}\right. \\ &\left.\times\exp\left[\frac{2\varepsilon(1+\alpha)}{\lambda}\right]\right]^{-1}.\end{aligned}$$

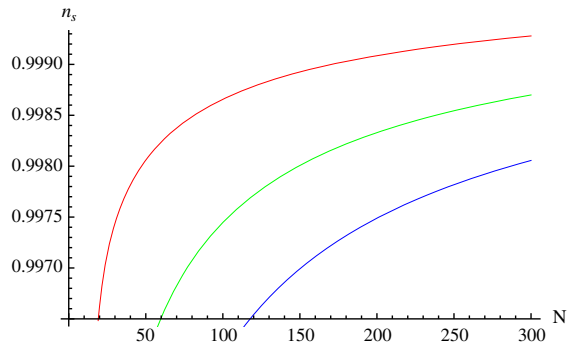

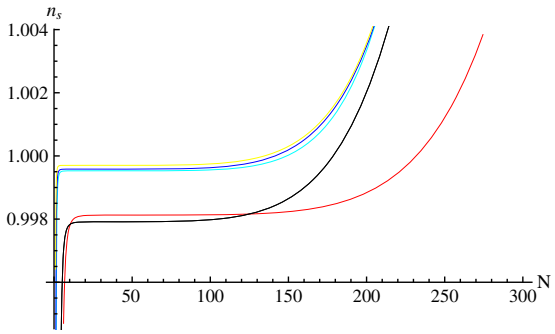

Fig. 2 *Left* n_s versus N for $A = 8.225 \times 10^2$, $\alpha = 0.775$, $\omega = -0.8$, $\lambda = 10$ (*red*), 50 (*green*), 70 (*blue*), $k = 1$ (*right*) graph for $A = 2.635 \times 10^2$, $\alpha = 0.81$, $\omega = -1.5$, $\lambda = 10$ (*red*), 50 (*zinc*), 70 (*purple*); $A = 8.407 \times 10^2$, $\alpha = 0.85$, $\omega = -1.7$, $\lambda = 10$ (*black*), 50 (*blue*), 70 (*yellow*) in the logamediate scenario

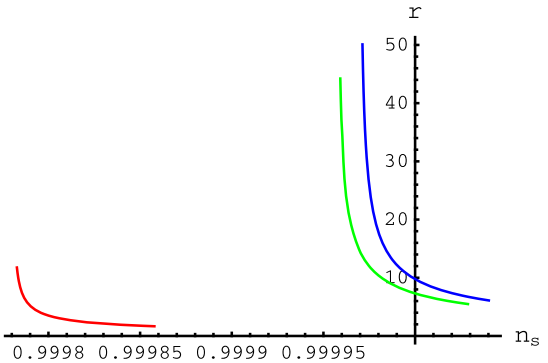

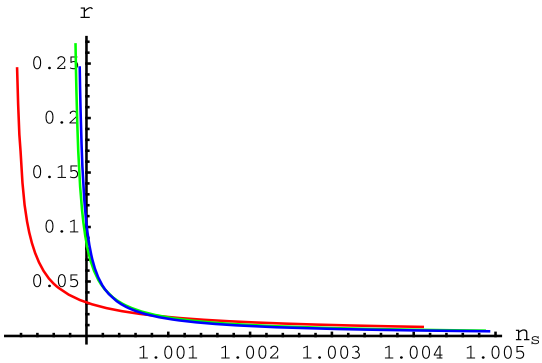

Fig. 3 Tensor–scalar ratio versus n_s in the logamediate scenario

The graphical behavior of n_s versus N for different values of the model parameters is shown in Fig. 2. The left graph shows that the spectral index is an increasing function of N, which confirms the compatibility of the model with recent observations. In the right graph, zinc, yellow, and blue curves correspond to $N = 0$ for $n_s \leq 1$. Consequently, for all choices of the free parameters, the model remains consistent with WMAP7 data. The tensor–scalar ratio becomes

$$r(N) = \frac{16(1-\lambda)}{A\lambda}\left(\frac{\kappa(A\lambda)^2}{3}\right)^{(\alpha+(1+\alpha)\psi)} \varepsilon^{\frac{1-2\lambda+2(\alpha+(1+\alpha)\psi)(\lambda-1)}{\lambda}} \times \exp\left[\varepsilon\left(\frac{1}{\lambda}-\frac{2}{\lambda}\alpha+(1+\alpha)\psi\right)\right] \times \left[1-\frac{A}{1+\omega}\left(\frac{\kappa}{3}\right)^{1+\alpha}(A\lambda)^{-2(1+\alpha)}\varepsilon^{\frac{-2(1+\alpha)}{\lambda}}\exp\left[\frac{2(1+\alpha)}{\lambda}\varepsilon\right]\right]^{\psi}.$$

During the logamediate scenario, Figs. 3 and 4 show a similar decreasing behavior for all possible choices of the model parameters. In all cases, we cannot have $n_s = 0.96$ in the allowed range of $r \leq 0.36$, which is compatible with WMAP7 data.

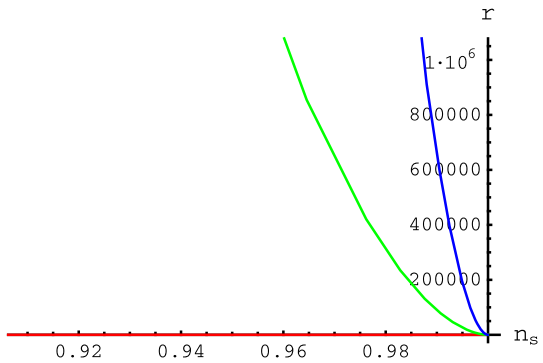

Fig. 4 Tensor–scalar ratio versus n_s in the logamediate scenario

3.2 Tachyon scalar field

In this section, we discuss the intermediate and logamediate inflationary scenarios in the presence of a tachyon scalar field.

3.2.1 Intermediate inflation

The solution of the tachyon field during the era of the intermediate scenario is given by Eq. (10),

$$\phi(t)=\left[\frac{2(1-f)}{3(Af)(1+\omega)}\right]^{\frac{1}{2}}\left[\frac{A}{(1+\omega)\left(\frac{3(Af)^2}{\kappa}\right)^{1+\alpha}\chi}\right]t^{\frac{\chi}{2}},$$

which gives

$$t=\left[\phi\left[\frac{3(Af)(1+\omega)}{2(1-f)}\right]^{\frac{1}{2}}\left[\frac{(1+\omega)\left(\frac{3(Af)^2}{\kappa}\right)^{1+\alpha}\chi}{A}\right]\right]^{\frac{2}{\chi}}, \tag{26}$$

where $\chi = f+2\alpha(f-1)-4(1+\alpha)(f-1)$. The scalar and tensor perturbed parameters in terms of N are

$$\begin{aligned}\mathcal{P}_{\mathcal{R}}&=\left(\frac{\kappa}{3}\right)^{\alpha}\left(\frac{\kappa}{8\pi^2}\right)\frac{(Af)^{3-2\alpha}}{(1-f)}(1+\omega)^{\frac{1}{2}}\mu^{\frac{(f-1)(3-2\alpha)}{f}}\\&\times\left[\left(\frac{3(Af)^2}{\kappa}\right)^{(1+\alpha)}\mu^{\frac{(f-1)(1+\alpha)}{f}}\frac{A}{1+\omega}\right]^{-\psi}\\&\times\left[1+\left(\frac{2}{\kappa}\right)\left(\frac{3}{\kappa}\right)^{\alpha}(Af)^{2\alpha+1}(f-1)\mu^{\frac{(f-1)(1+2\alpha)}{f}}\right.\\&\left.\times\left[\left(\frac{3(Af)^2}{\kappa}\right)^{1+\alpha}\mu^{\frac{(f-1)(1+\alpha)}{f}}-\frac{A}{1+\omega}\right]^{-1}\right]^{-\frac{1}{2}},\\\mathcal{P}_g&=\left(\frac{2\kappa}{\pi^2}\right)(Af)^2\mu^{\frac{2(f-1)}{f}}.\end{aligned}$$

The corresponding scalar spectral index is

$$\begin{aligned}n_s-1=&\frac{(1-f)(3-2\alpha)}{Af}\mu^{-1}-\left(\frac{3}{\kappa}\right)^{1+\alpha}(1+\alpha)(f-1)(Af)^{1+2\alpha}\\&\times\mu^{\frac{(f-1)(1+\alpha)}{f}-1}\\&\times\left[\mu^{\frac{(f-1)(1+\alpha)}{f}}\left(\frac{3(Af)^2}{\kappa}\right)^{1+\alpha}-\frac{A}{1+\omega}\right]^{-1}\\&-\frac{1}{2}\left[1+\left(\frac{2}{\kappa}\right)\left(\frac{3}{\kappa}\right)^{\alpha}(f-1)\right.\\&\times(Af)^{1+2\alpha}\mu^{\frac{(f-1)(1+2\alpha)}{f}}\\&\left.\times\left[\left(\frac{3(Af)^2}{\kappa}\right)^{1+\alpha}\mu^{\frac{(f-1)(1+\alpha)}{f}}\frac{A}{1+\omega}\right]^{-1}\right]^{-1}\\&-\left[\left(\frac{2}{\kappa}\right)\left(\frac{3(Af)^2}{\kappa}\right)^{\alpha}(f-1)^2(1+2\alpha)\mu^{\frac{2\alpha(f-1)-1}{f}}\right.\\&\times\left[\left(\frac{3}{\kappa}\right)^{1+\alpha}(Af)^{2(1+\alpha)}\mu^{\frac{(f-1)(1+\alpha)}{f}}\right.\\&\left.\left.-\frac{A}{1+\omega}\right]^{-1}\left(\frac{2}{\kappa}\right)\left(\frac{3}{\kappa}\right)^{1+2\alpha}(Af)^{2(1+2\alpha)}\right.\\&\times(1-f)^2(1+\alpha)\mu^{\frac{(f-1)(2+3\alpha)-f}{f}}\\&\left.\times\left[\left(\frac{3}{\kappa}\right)^{1+\alpha}(Af)^{2(1+\alpha)}\mu^{\frac{(f-1)(1+\alpha)}{f}}-\frac{A}{1+\omega}\right]^{-2}\right].\end{aligned} \tag{27}$$

From $\mathcal{P}_{\mathcal{R}}$ and $\mathcal{P}_g$, we find the tensor–scalar ratio as

$$\begin{aligned}r(N)=&16\left(\frac{3}{\kappa}\right)^{\alpha}(1+\omega)^{-\frac{1}{2}}(1-f)(Af)^{2\alpha-1}\mu^{\frac{(f-1)(2\alpha-1)}{f}}\\&\times\left[\left(\frac{3}{\kappa}\right)^{1+\alpha}(Af)^{2(1+\alpha)}\mu^{\frac{(f-1)(1+\alpha)}{f}}-\frac{A}{1+\omega}\right]^{\psi}\\&\times\left[1+\left(\frac{2}{\kappa}\right)\left(\frac{3}{\kappa}\right)^{\alpha}(f-1)(Af)^{1+2\alpha}\mu^{\frac{(f-1)(1+2\alpha)}{f}}\right.\\&\left.\times\left[\left(\frac{3}{\kappa}\right)^{1+\alpha}(Af)^{2(1+\alpha)}\mu^{\frac{(f-1)(1+\alpha)}{f}}-\frac{A}{1+\omega}\right]^{-1}\right]^{\frac{1}{2}}.\end{aligned}$$

The left graph of Fig. 5 represents an increasing behavior for all four choices of the parameters. In this case, the value of $n_s = 0.96$ corresponds to $N \approx 20$ (red), 50 (zinc), 70 (blue), 90 (green). Thus the GCCG inflationary intermediate model with the tachyon field is compatible with the WMAP7 data. The right graph of Fig. 5 shows that the curves in the r–n_s plane are decreasing, which indicates incompatibility of this model with recent observations. The physically acceptable range of the tensor–scalar ratio is not attained at $n_s = 0.96$ during the era of the intermediate scenario using the tachyon field.

3.2.2 *Logamediate inflation*

Using the logamediate scale factor in Eq. (10), we have

$$\phi(t)-\phi(t_0)=\left[\left(\frac{2}{\kappa}\right)\left(\frac{3}{\kappa}\right)^{\alpha}\frac{\lambda-1}{1+\omega}(A\lambda)^{1+2\alpha}\right]^{\frac{1}{2}}\Xi(t), \tag{28}$$

which provides t in terms of ϕ (by assuming $\phi(t_0)=0$) as

$$t=\Xi^{-1}\left[\left[\left(\frac{2}{\kappa}\right)\left(\frac{3}{\kappa}\right)^{\alpha}\frac{\lambda-1}{1+\omega}(A\lambda)^{1+2\alpha}\right]^{-\frac{1}{2}}\phi\right].$$

The scalar as well as tensor power spectra can be expressed as

$$\begin{aligned}\mathcal{P}_{\mathcal{R}}=&\left(\frac{\kappa}{3}\right)^{\alpha}\left(\frac{\kappa}{8\pi^2}\right)\frac{(1+\omega)^{\frac{1}{2}}}{1-\lambda}(A\lambda)^{3-2\alpha}\varepsilon^{\frac{3\lambda-2\alpha(\lambda-1)-2}{\lambda}}\\&\times\exp\left[\frac{2\varepsilon(\alpha-1)}{\lambda}\right]\left[\left(\frac{3}{\kappa}\right)^{1+\alpha}(A\lambda)^{2(1+\alpha)}\varepsilon^{\frac{2(1+\alpha)(\lambda-1)}{\lambda}}\right.\\&\left.\times\exp\left[\frac{-2\varepsilon(1+\alpha)}{\lambda}\right]-\frac{A}{1+\omega}\right]^{1-\psi},\\\mathcal{P}_g=&\left(\frac{2\kappa}{\pi^2}\right)(A\lambda)^2\varepsilon^{\frac{2(\lambda-1)}{\lambda}}\exp\left[-\frac{2\varepsilon}{\lambda}\right].\end{aligned}$$

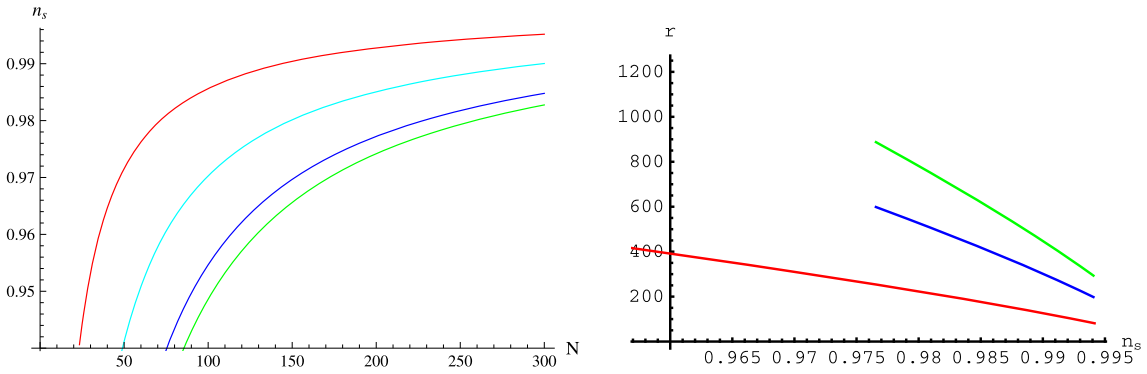

Fig. 5 *Left* n_s versus N, *right* tensor–scalar ratio versus n_s in the intermediate scenario

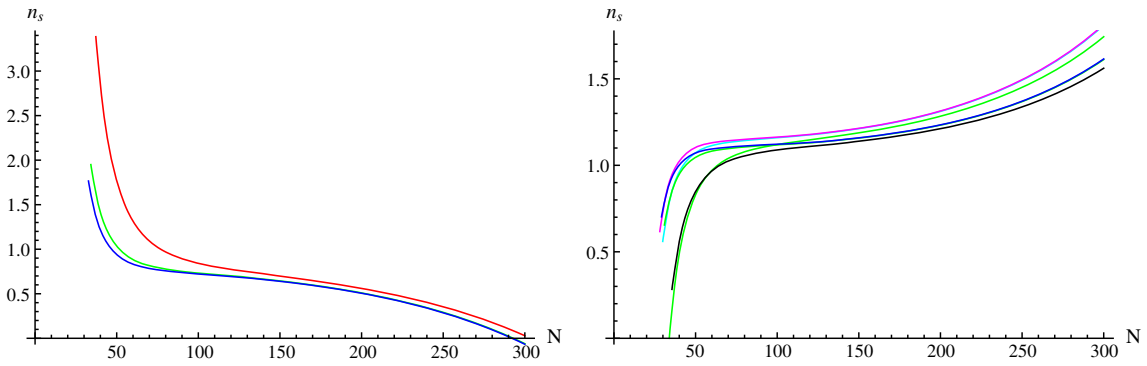

Fig. 6 n_s versus N in the logamediate scenario

The scalar spectral index has the form

$$
\begin{aligned}
n_s - 1 = {} & \left(\frac{3\lambda - 2\alpha(\lambda-1) - 2}{A\lambda}\right)\varepsilon^{-1} + \frac{2(\alpha-1)}{A\lambda} \\
& + 2(1-\psi)(1+\alpha)(\lambda-1)\left(\frac{3}{\kappa}\right)^{1+\alpha} \\
& \times (A\lambda)^{2\alpha-1}\left[\left(\frac{3}{\kappa}\right)^{1+\alpha}(A\lambda)^{2(1+\alpha)}\varepsilon^{\frac{2(1+\alpha)(\lambda-1)}{\lambda}}\right. \\
& \left. \times \exp\left[\frac{-2(1+\alpha)}{\lambda}\varepsilon\right] - \frac{A}{1+\omega}\right]^{-1} \\
& \times \varepsilon^{\frac{2(1+\alpha)(\lambda-1)}{\lambda}-1} + \frac{1}{1-\lambda} \\
& \times \exp\left[\frac{-2(1+\alpha)}{\lambda}\left[\frac{N}{A} + (A\lambda)^{\frac{\lambda}{1-\lambda}}\right]\right].
\end{aligned}
$$

The left and right graphs of Fig. 6 show opposite behavior to each other for different values of λ. In the left graph, when λ increases, n_s decreases as N increases for all three curves and the constrained $n_s = 0.96$ corresponds to $N \approx 50$ for green and blue curves, while $N \approx 100$ for the red one. The right graph shows increasing trajectories and $n_s = 0.96$ lies in the region $N < 50$ for all choices of the model parameters.

The tensor–scalar ratio is

$$
\begin{aligned}
r(N) = {} & -16\left(\frac{3}{\kappa}\right)^{1+\alpha}\frac{(\lambda-1)}{(\omega+1)^{\frac{1}{2}}}(A\lambda)^{2\alpha-1}\varepsilon^{\frac{2\alpha(\lambda-1)-\lambda}{\lambda}} \\
& \times \exp\left[\frac{-2\varepsilon(\alpha+4)}{\lambda}\right]\left[\left(\frac{3(A\lambda)^2}{\kappa}\right)^{1+\alpha}\varepsilon^{\frac{2(1+\alpha)(\lambda-1)}{\lambda}}\right. \\
& \left. \times \exp\left[\frac{-2\varepsilon(1+\alpha)}{\lambda}\right] - \frac{A}{1+\omega}\right]^{\psi+1}.
\end{aligned}
$$

The two graphs of Fig. 7 show a similar behavior as increasing λ leads to increasing r–n_s trajectories. The red curve in both graphs indicates that $r = 0$ for $n_s = 0.96$, which is incompatible according to WMAP7 data. Figure 8 shows a decreasing behavior with increasing λ. In this case, $n_s = 0.96$ corresponds to $r = 0$ for $\lambda = 50,\ 70$, while the red curve ($\lambda = 10$) does not lie in the region $r < 0.36$.

4 Concluding remarks

In this paper, we have discussed the GCCG inflationary universe model for a flat FRW geometry during the eras of the intermediate as well as logamediate scenarios. The standard and tachyon scalar fields are considered as the matter con-

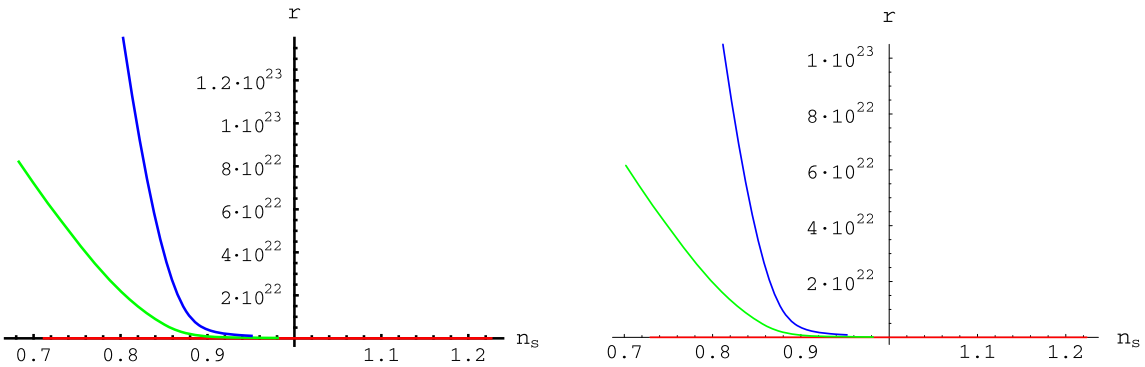

Fig. 7 The left graph of the tensor–scalar ratio versus n_s in the logamediate scenario

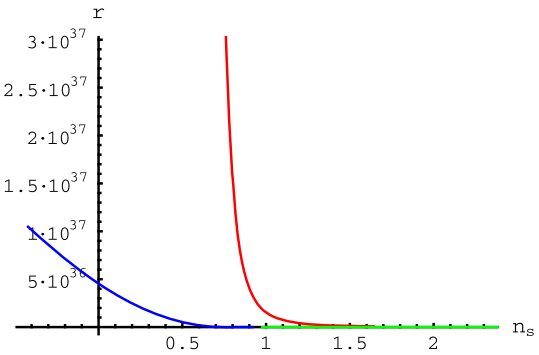

Fig. 8 Tensor–scalar ratio versus n_s in the logamediate scenario

tent of this universe. In order to study Chaplygin inspired inflation, we have modified the first Friedmann equation by applying the slow-roll approximation and found solutions of the scalar fields as well as their corresponding potentials. We have also evaluated the slow-roll parameters, the number of e-folds, scalar and tensor power spectra, the scalar index, and finally the important parameter of the tensor–scalar ratio, which is constrained by WMAP7 data. We have checked the physical compatibility of our model with the WMAP7 results, i.e., the standard value $n_s = 0.96$ must be found in the region $r < 0.36$. The N–n_s and r–n_s trajectories are plotted to explore the behavior of these parameters in each case.

By constraining $0.96 \leq n_s \leq 1.002$ and $\mathcal{P}_{\mathcal{R}}(k_0 = 0.002\ \mathrm{Mpc}^{-1}) = (2.445 \pm 0.096) \times 10^{-9}$, according to the observations of WMAP7, we obtain the following values of the model parameter: $A = 8.225 \times 10^2,\ 2.635 \times 10^2,\ 8.407 \times 10^2$ for $\alpha = 0.775,\ 0.81,\ 0.85$, $\omega = -0.8, -1.5, -1.7$, $g = \frac{1}{2}$, $\kappa = 1$ from Eq. (21). Using these values, we plot the graph of N and r versus n_s in the intermediate and logamediate scenarios. The left graph of Fig. 1 shows that $n_s = 0.96$ corresponds to $N = 20$ for all possible choices of the model parameters during the intermediate era. The right panel of Fig. 1 shows that none of the cases is compatible with WMAP7 data as the observed value $0.96 \leq n_s \leq 1$ does not lie in the region $r \leq 0.36$. The graphical analysis of the intermediate era represents incompatibility of the considered inflationary universe model for standard scalar field with WMAP7 data. During the logamediate era, the left and right panels of Fig. 2 represent similar increasing trajectories of N–n_s with the increase and decrease of the model parameters, $\lambda = 10,\ 50,\ 70$, respectively. Thus the number of e-folds remains consistent with the observational value of n_s according to the WMAP7 data. On the other hand, Figs. 3 and 4 show similar decreasing behaviors for all possible choices of the model parameters. The graphical analysis of this observational parameter of interest, r versus n_s, shows a violation of the observed value of WMAP7 (as $n_s = 0.96$ does not correspond to $r \leq 0.36$). Thus we conclude that the GCCG inflationary universe model with a standard scalar field remains incompatible with observational data of WMAP7.

For the tachyon field of the inflationary universe, the left plot of Fig. 5 represents an increasing behavior of N with respect to n_s for all four choices of the parameters. In this case, N remains consistent with the observational value of n_s as for the standard scalar field. The right graph of Fig. 5 shows the incompatibility of this inflationary model with recent observations of WMAP7 by decreasing r–n_s trajectories. In the logamediate era, the left and right graphs of Fig. 6 are opposite in nature for different values of λ. In the left panel, n_s–N decreases with the increase of λ, while the right panel shows increasing trajectories and $n_s = 0.96$ lies in the region $N < 50$ for all choices of the model parameters. Figures 7 and 8 show similar behaviors as obtained for the standard scalar field during the logamediate era, i.e., increasing λ leads to decreasing r–n_s trajectories. In this case, the red curve in both graphs matches (i.e., for $n_s = 0.96,\ r = 0$), which is not a physical value of r according to the WMAP7 data. We conclude that the inflationary universe model remains incompatible with WMAP7 data for standard and tachyon scalar fields, both in the intermediate and the logamediate scenarios. Thus the accelerating expansion of the universe cannot be achieved by using the GCCG

inflationary universe model in both intermediate and logamediate regimes.

It is worth mentioning here that all the results for the intermediate regime with standard and tachyon scalar fields reduce to [38]. Our results for this model support the results of [47] that this model is less effective as compared to MCG and other DE models.

Acknowledgments We would like to thank the Higher Education Commission, Islamabad, Pakistan, for its financial support through the *Indigenous Ph.D. Fellowship for 5K Scholars, Phase-II, Batch-I.*

References

1. S. Perlmutter et al., Nature **391**, 51 (1998)
2. A.G. Riess et al., Astron. J. **116**, 1009 (1998)
3. B. Ratra, P.J.E. Peebles, Phys. Rev. D **37**, 3406 (1998)
4. T. Chiba, T. Okabe, M. Yamaguchi, Phys. Rev. D **62**, 023511 (2000)
5. T. Padmanabhan, Phys. Rev. D **66**, 021301 (2002)
6. Z.K. Guo et al., Phys. Lett. B **608**, 177 (2005)
7. V. Gorini, A. Kamenshchik, U. Moschella, Phys. Rev. D **67**, 063509 (2003)
8. B. Hu, Y. Ling, Phys. Rev. D **73**, 123510 (2006)
9. M.R. Setare, J. Cosmol. Astropart. Phys. **0701**, 023 (2007)
10. W. Zimdahl, J.C. Fabris, Class. Quant. Grav. **22**, 4311 (2005)
11. D. Bazeia, Phys. Rev. D **59**, 085007 (1999)
12. U. Debnath, A. Banerjee, S. Chakraborty, Class. Quant. Grav. **21**, 5609 (2004)
13. P.F. González-Diaz, Phys. Rev. D **68**, 021303 (2003)
14. A. Kamenshchik, U. Moschella, V. Pasquier, Phys. Lett. B **511**, 265 (2001)
15. A. Sen, Mod. Phys. Lett. A **17**, 1797 (2002)
16. M. Sami, P. Chingangbam, T. Qureshi, Phys. Rev. D **66**, 043530 (2002)
17. G.W. Gibbons, Phys. Lett. B **537**, 1 (2002)
18. M.C. Bento, O. Bertolami, A. Sen, Phys. Rev. D **66**, 043507 (2002)
19. A. Dev, J.S. Alcaniz, D. Jain, Phys. Rev. D **67**, 023515 (2003)
20. P.F. González-Diaz, Phys. Lett. B **562**, 1 (2003)
21. G.M. Kremer, Gen. Relat. Grav. **35**, 1459 (2003)
22. R. Bean, O. Dore, Phys. Rev. D **68**, 023515 (2003)
23. L.P. Chimento, Phys. Rev. D **69**, 123517 (2004)
24. O. Bertolami, V. Duvvuri, Phys. Lett. B **640**, 121 (2006)
25. S. del Campo, R. Herrera, Phys. Lett. B **660**, 282 (2008)
26. S. del Campo, R. Herrera, Phys. Lett. B **665**, 100 (2008)
27. G.A. Monerat et al., Phys. Rev. D **76**, 024017 (2007)
28. A.A. Starobinsky, Phys. Lett. B **91**, 99 (1980)
29. A. Guth, Phys. Rev. D **23**, 347 (1981)
30. B. Gold et al., Astrophys. J. Suppl. **192**, 15 (2011)
31. J. Yokoyama, K. Maeda, Phys. Lett. B **207**, 31 (1988)
32. M.R. Setare, V. Kamali, Gen. Relat. Grav. **46**, 1642 (2014)
33. P.G. Ferreira, M. Joyce, Phys. Rev. D **58**, 023503 (1998)
34. J.D. Barrow, N.J. Nunes, Phys. Rev. D **76**, 043501 (2007)
35. M.R. Setare, V. Kamali, arXiv:1309.2452
36. M. Sharif, R. Saleem, Eur. Phys. J. C **74**, 2738 (2014)
37. M. Sharif, R. Saleem, Astropart. Phys. (to be appeared, 2014)
38. R. Herrera, M. Olivares, N. Videla, Eur. Phys. J. C **73**, 2295 (2013)
39. J.D. Barrow, A.R. Liddle, Phys. Rev. D **47**, 5219 (1993)
40. A.A. Starobin-sky, J. Exp. Theor. Phys. Lett. **82**, 169 (2005)
41. S. del Campo, R. Herrera, J. Saavedra, C. Campuzano, E. Rojas, Phys. Rev. D **80**, 123531 (2009)
42. R. Herrera, N. Videla, Eur. Phys. J. C **67**, 499 (2010)
43. J. Martin, D.J. Schwarz, Phys. Rev. D **57**, 3302 (1998)
44. R. Zarrouki, M. Bennai, Phys. Rev. D **82**, 123506 (2010)
45. A. Liddle, D. Lyth, *Cosmological inflation and large-scale structure* (Cambridge University Press, Cambridge, 2000)
46. M.R. Garousi, M. Sami, S. Tsujikawa, Phys. Rev. D **70**, 043536 (2004)
47. P. Rudra, Astrophys. Space Sci. **342**, 579 (2012)